

# Cholesterol Regulates Syntaxin 6 Trafficking at *trans*-Golgi Network Endosomal Boundaries

Meritxell Reverter,<sup>1,11</sup> Carles Rentero,<sup>1,11</sup> Ana Garcia-Melero,<sup>1</sup> Monira Hoque,<sup>2</sup> Sandra Vilà de Muga,<sup>1</sup> Anna Álvarez-Guaita,<sup>1</sup> James R.W. Conway,<sup>3</sup> Peta Wood,<sup>2</sup> Rose Cairns,<sup>2</sup> Lilia Lykopoulou,<sup>4</sup> Daniel Grinberg,<sup>5</sup> Lluïsa Vilageliu,<sup>5</sup> Marta Bosch,<sup>6</sup> Joerg Heeren,<sup>7</sup> Juan Blasi,<sup>8</sup> Paul Timpson,<sup>3</sup> Albert Pol,<sup>1,6,9</sup> Francesc Tebar,<sup>1,6</sup> Rachael Z. Murray,<sup>10</sup> Thomas Grewal,<sup>2,\*</sup> and Carlos Enrich<sup>1,6,\*</sup>

<sup>1</sup>Departament de Biologia Cel·lular, Immunologia i Neurociències, Facultat de Medicina, Universitat de Barcelona, 08036 Barcelona, Spain

<sup>2</sup>Faculty of Pharmacy, University of Sydney, Sydney, NSW 2006, Australia

<sup>3</sup>Garvan Institute of Medical Research and Kinghorn Cancer Centre, Cancer Research Program, St. Vincent's Clinical School, Faculty of Medicine, University of New South Wales, Sydney, NSW 2010, Australia

<sup>4</sup>First Department of Pediatrics, University of Athens, Aghia Sofia Children's Hospital, 11527 Athens, Greece

<sup>5</sup>Departament de Genètica, Facultat de Biologia, Universitat de Barcelona, CIBERER, IBUB, 08028 Barcelona, Spain

<sup>6</sup>Centre de Recerca Biomèdica CELLEX, Institut d'Investigacions Biomèdiques August Pi i Sunyer (IDIBAPS), 08036 Barcelona, Spain

<sup>7</sup>Department of Biochemistry and Molecular Biology II, Molecular Cell Biology, University Medical Center Hamburg-Eppendorf, 20246 Hamburg, Germany

<sup>8</sup>Department of Pathology and Experimental Therapeutics, IDIBELL-University of Barcelona, L'Hospitalet de Llobregat, 08907 Barcelona, Spain

<sup>9</sup>Institució Catalana de Recerca i Estudis Avançats (ICREA), 08010 Barcelona, Spain

<sup>10</sup>Tissue Repair and Regeneration Program, Institute of Health and Biomedical, Innovation, Queensland University of Technology, Brisbane, QLD 4095, Australia

<sup>11</sup>Co-first author

\*Correspondence: [thomas.grewal@sydney.edu.au](mailto:thomas.grewal@sydney.edu.au) (T.G.), [enrich@ub.edu](mailto:enrich@ub.edu) (C.E.)

<http://dx.doi.org/10.1016/j.celrep.2014.03.043>

This is an open access article under the CC BY-NC-ND license (<http://creativecommons.org/licenses/by-nc-nd/3.0/>).

## SUMMARY

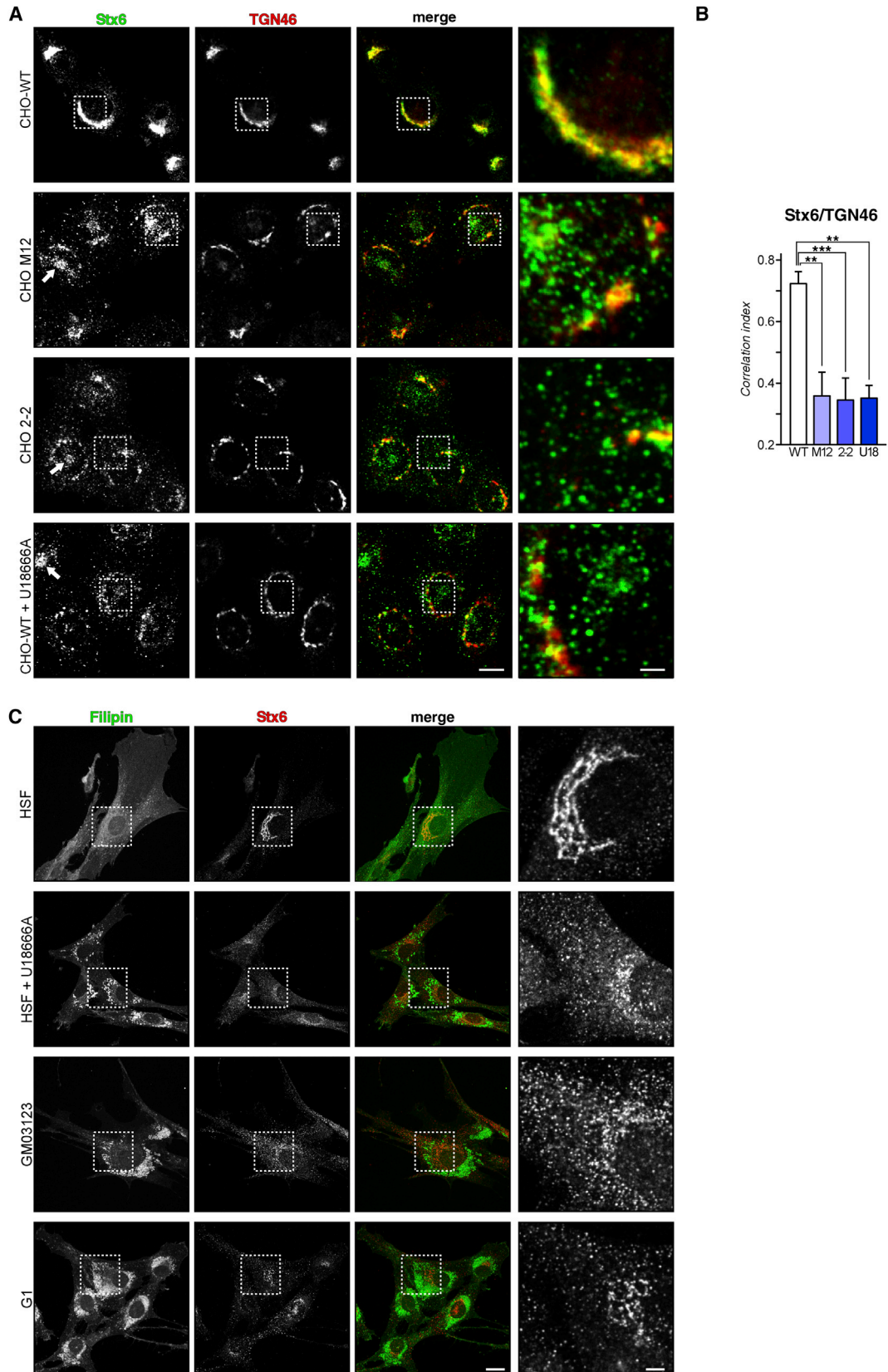
Inhibition of cholesterol export from late endosomes causes cellular cholesterol imbalance, including cholesterol depletion in the *trans*-Golgi network (TGN). Here, using Chinese hamster ovary (CHO) Niemann-Pick type C1 (NPC1) mutant cell lines and human NPC1 mutant fibroblasts, we show that altered cholesterol levels at the TGN/endosome boundaries trigger Syntaxin 6 (Stx6) accumulation into VAMP3, transferrin, and Rab11-positive recycling endosomes (REs). This increases Stx6/VAMP3 interaction and interferes with the recycling of  $\alpha$ V $\beta$ 3 and  $\alpha$ 5 $\beta$ 1 integrins and cell migration, possibly in a Stx6-dependent manner. In NPC1 mutant cells, restoration of cholesterol levels in the TGN, but not inhibition of VAMP3, restores the steady-state localization of Stx6 in the TGN. Furthermore, elevation of RE cholesterol is associated with increased amounts of Stx6 in RE. Hence, the fine-tuning of cholesterol levels at the TGN-RE boundaries together with a subset of cholesterol-sensitive SNARE proteins may play a regulatory role in cell migration and invasion.

## INTRODUCTION

The intracellular trafficking, distribution, and concentration of cellular cholesterol contributes to regulate lipid and protein

transport between cellular compartments and organizes membrane microdomains, such as lipid rafts, at the plasma membrane and in endo-/exocytic pathways (Maxfield and van Meer, 2010; Simons and Ikonen, 2000). In general, cells obtain cholesterol through endocytosis of low-density lipoproteins (LDLs). The subsequent delivery of LDL cholesterol to endolysosomes and then to other subcellular compartments is facilitated by a complex transport machinery, consisting of vesicular and nonvesicular pathways (Ikonen, 2008; Mesmin and Maxfield, 2009). Deregulation of these cholesterol transport pathways is associated with human disorders, including lysosomal storage diseases, neurological disorders, and cardiovascular events (Ikonen, 2006).

In the context of membrane trafficking, cholesterol is also essential for the functioning of a subset of SNARE proteins along secretory and endocytic pathways. We and others showed that cholesterol modulates the clustering and the location of several SNARE proteins in membranes, such as the t-SNARE SNAP23 and Stx4 (Reverter et al., 2011) or SNAP25 and Stx1A (Lang et al., 2001; Veale et al., 2011). Syntaxin 6 (Stx6) is another t-SNARE linked to cholesterol transport, contributing to the delivery of lipids and proteins required for caveolae endocytosis (Choudhury et al., 2006). Stx6 is a cholesterol-binding protein (Hulce et al., 2013), predominantly localized at the *trans*-Golgi network (TGN) (Bock et al., 1997) involved in the regulation of cholesterol-rich domains that determine the levels of cell-surface-associated  $\alpha$ 5 $\beta$ 1 integrin, focal adhesion kinase (FAK), focal adhesion sites, and directional migration toward fibronectin (FN) (Tiwari et al., 2011). However, how cholesterol affects Stx6-dependent trafficking mechanisms still remains unclear.



(legend on next page)

Several SNAREs have been implicated in integrin trafficking and related to the migratory ability of cells. Cholesterol controls  $\alpha$ V $\beta$ 3 integrin signal complex formation (Green et al., 1999), cell adhesion, and migration onto FN (Ramprasad et al., 2007). This includes VAMP2/VAMP3, Stx3/Stx4, and SNAP23 participating in  $\beta$ 1 integrin recycling (Day et al., 2011; Powelka et al., 2004; Proux-Gillardeaux et al., 2005; Skalski and Coppelino, 2005; Veale et al., 2010) and VAMP3 together with Stx6 determining cell-surface-associated levels of  $\alpha$ 5 $\beta$ 1 integrin and FAK (Riggs et al., 2012; Tiwari et al., 2011).

Integrins are cell-surface receptors that mediate and coordinate cellular responses to the extracellular matrix (ECM). Integrins display their principal functions at the plasma membrane but reside and traffic through the endocytic compartment, in particular in recycling endosomes (RE) (Jones et al., 2006; Pellinen and Ivaska, 2006). Certain integrin receptors, such as  $\alpha$ V $\beta$ 3, are recycled rapidly to the plasma membrane through a short loop, whereas  $\alpha$ 5 $\beta$ 1 returns to the cell surface through a transitory recycling compartment (long-loop) (Roberts et al., 2001).

The recycling of integrins depends upon many endocytic regulatory proteins that also control the transport of other internalized receptors. For instance, the guanosine triphosphate (GTP)-binding proteins Rab4 (Roberts et al., 2001), Rab11, Arf6 (Powelka et al., 2004), Rab21, Rab5 (Pellinen et al., 2006), and more recently Rab25 (Dozynkiewicz et al., 2012) have been implicated in integrin recycling. Based on these studies, other regulators of endocytic recycling and/or proteins (SNAREs) or lipids that physically and/or functionally interact with certain Rab proteins could play a role in the regulation of integrin trafficking.

Using Niemann-Pick type C1 (NPC1) mutant Chinese hamster ovary (CHO) cell lines (CHO M12 and CHO 2-2) (Dahl et al., 1992; Millard et al., 2000), pharmacological U18666A treatment (Liscum and Faust, 1989), and loss-of-function mutant NPC1-P692S (Du et al., 2011; Millard et al., 2005; Ohgami et al., 2004), all of which are models shown to accumulate cholesterol in late endosomes (LE) with concomitant cholesterol depletion in Golgi membranes, we provide insights into how cholesterol pools at the Golgi/endosomal boundaries regulate cell migration. Mechanistically, diminution of Golgi cholesterol perturbs trafficking between RE and TGN to trigger Stx6 accumulation in Rab11-containing RE. This correlates with a diminished cell-surface expression of integrins in NPC1 mutant models leading to reduced cell migration and invasion in two- and three-dimensional environments.

Implicating physiological relevance, the human NPC1 mutant fibroblast cell line (GM03123; Choudhury et al., 2004) and primary fibroblasts from a NPC1 patient (G1) (Rodríguez-Pascual et al., 2012) display translocation of Stx6 into RE, as well as diminished cell-surface expression of  $\alpha$ V,  $\alpha$ 5, and  $\beta$ 3 integrins

and, consequently, reduced cell migration. This study provides evidence that modulation of cholesterol levels at the interface of TGN and RE determines Stx6 localization and ability to interact with VAMP4 or VAMP3, thereby possibly regulating cell migration through Stx6-dependent  $\alpha$ V $\beta$ 3 and  $\alpha$ 5 $\beta$ 1 integrin trafficking.

## RESULTS

### Cholesterol-Dependent Stx6 Translocation into Rab11/VAMP3-Recycling Endosomes

NPC1 mutant cell lines CHO M12 and CHO 2-2 or U18666A-treated wild-type CHO (CHO-WT) cells are well characterized for their cholesterol accumulation in LE, as judged by filipin-positive LE structures (Figure S1). Impaired LE cholesterol (LE-chol) export leads to a reduction of Golgi cholesterol (Blanchette-Mackie et al., 1988; Coxey et al., 1993), interferes with post-Golgi transport (Cubells et al., 2007, 2008; Pol et al., 2005; Reverter et al., 2011; Wang et al., 2000), and sequesters the t-SNAREs SNAP23 and Stx4 in the Golgi (Reverter et al., 2011). Here, we investigated if cholesterol imbalance could affect localization and function of another member of the SNARE family, Stx6, which has been linked to cholesterol and caveolin transport (Choudhury et al., 2006; Urano et al., 2008).

In CHO-WT cells, Stx6 was located in perinuclear TGN membranes, where the vast majority of Stx6 colocalizes with the Golgi marker TGN46 (Figure 1A) (Bock et al., 1997; Choudhury et al., 2006) and with VAMP4, a v-SNARE predominantly localized in the TGN (see Figures 5A and 5B). In addition, a distinct population of Stx6 vesicles not colocalizing with TGN46 and probably representing early endosomes (EE) and/or secretory structures was observed.

In contrast, Stx6 was predominantly located in scattered cytoplasmic structures in CHO M12 and CHO 2-2 as well as U18666A-treated CHO-WT cells (Figure 1A; see quantification in Figure 1B). In addition, approximately 30%–40% of these NPC1 mutant cell lines also contained Stx6 in sometimes prominent, perinuclear recycling endosomes (perinuclear recycling endosomal compartment [PNRE], arrows). Importantly, this Stx6-positive compartment did not colocalize with TGN46 or VAMP4 but contained internalized transferrin and endogenous Rab11 (see below), indicative of the recycling compartment.

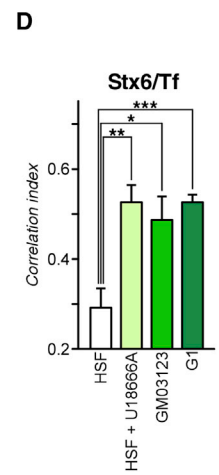
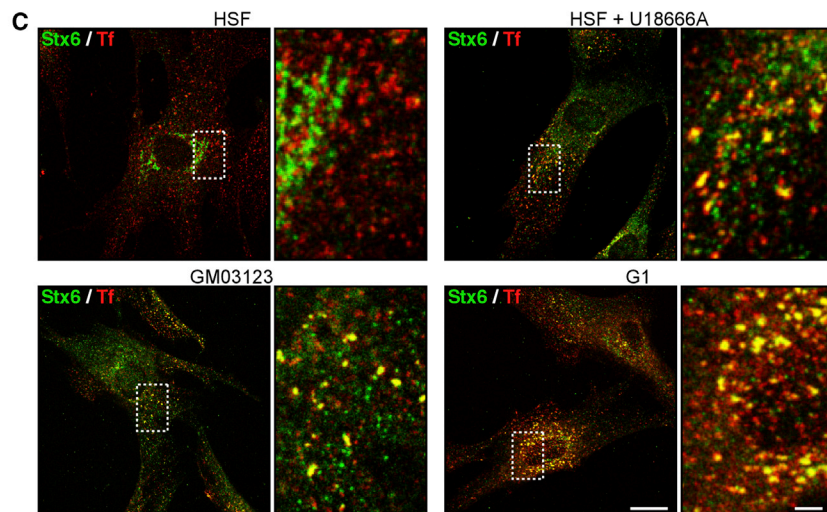
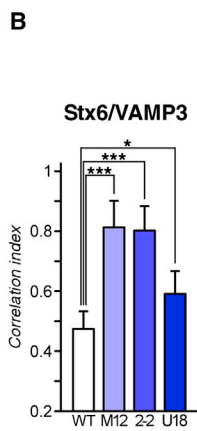
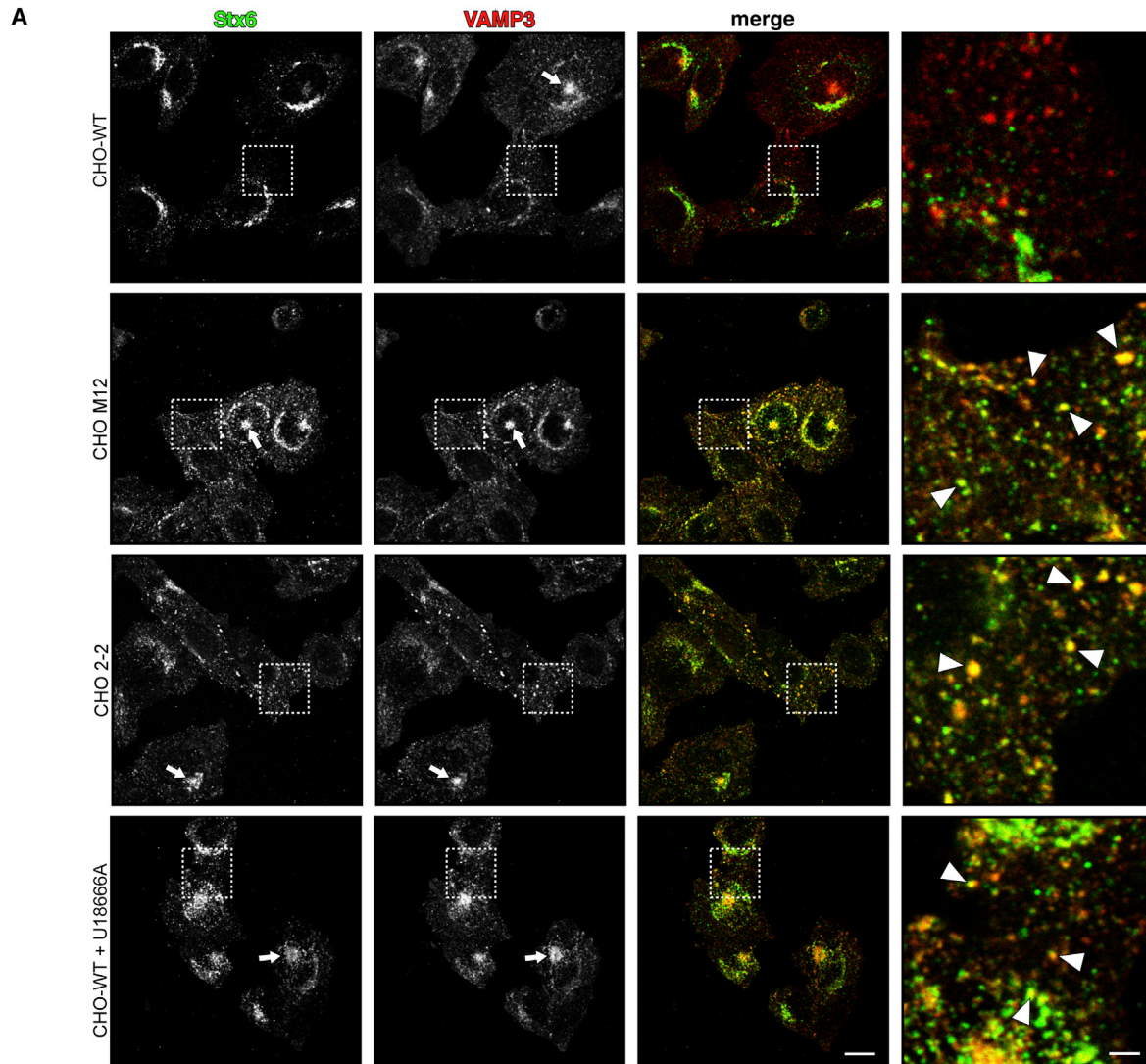
Similarly, in human skin fibroblasts (HSF), most of Stx6 labeling consisted of a distinctive perinuclear network of Golgi membranes (Figure 1C), whereas Stx6 was predominantly located in scattered punctate structures in the NPC1 mutant GM03123 cell line; in primary fibroblasts from a NPC1 patient, NPC1-G1 (G1); and in U18666A-treated HSF fibroblasts. The loss of Golgi-associated Stx6 was not due to alterations in Golgi morphology in NPC1 mutant models or human NPC1

### Figure 1. Stx6 Localization in NPC1 Mutant Cells

(A) CHO-WT, CHO M12, CHO 2-2, and U18666A-treated CHO-WT cells were fixed and immunolabeled with anti-Stx6 (green) and anti-TGN46 (red). Representative images and insets (right panels) show Stx6 staining details at the Golgi and in perinuclear recycling endosomes (PNRE, arrows) in NPC1 mutant cell lines or U18666A-treated cells. The scale bars represent 10 and 2  $\mu$ m (insets).

(B) Quantification of Stx6/TGN46 colocalization using the correlation index (see the Experimental Procedures).

(C) Stx6 localization in human skin fibroblasts (HSF), U18666A-treated HSF, and G03123 and G1 fibroblasts. Cells were immunolabeled with anti-Stx6 (red) and stained with filipin. The scale bars represent 20 and 5  $\mu$ m (insets).



(legend on next page)

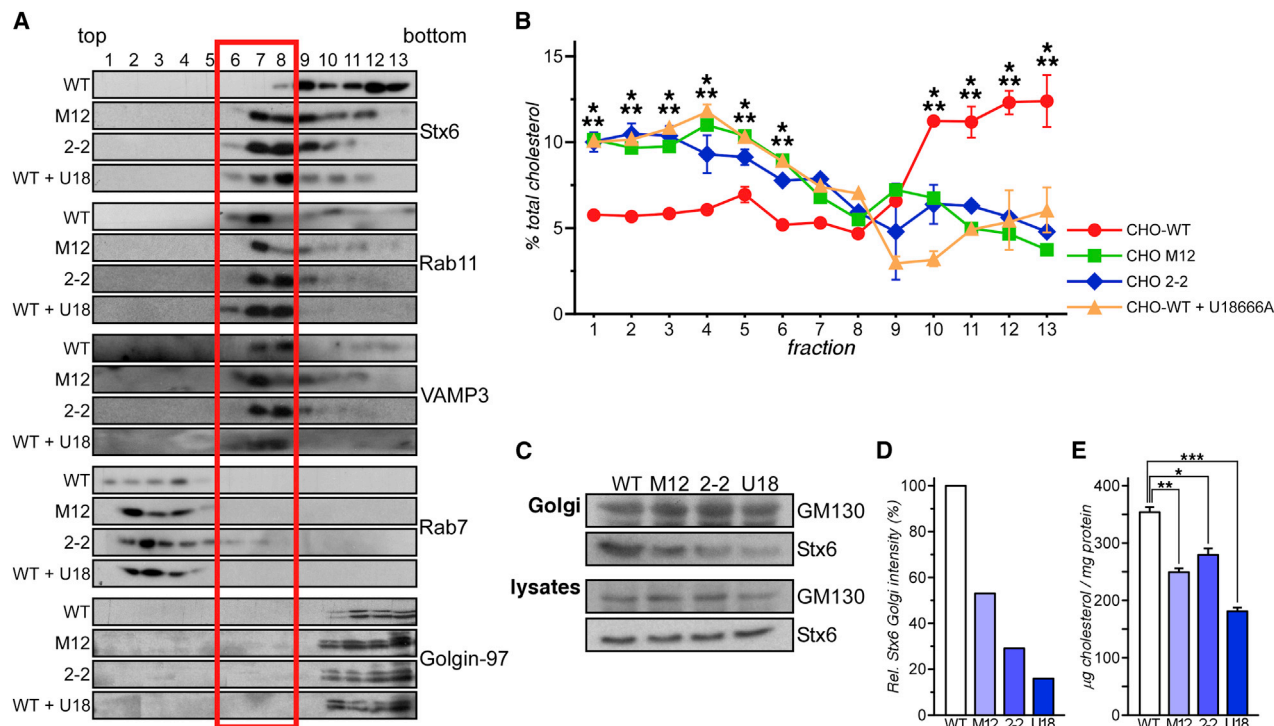


**Figure 3. Biochemical Characterization of Endosomal and Golgi Subcellular Fractions**

(A) Cellular fractions of a discontinuous sucrose gradient of CHO-WT, CHO M12, CHO 2-2, and CHO-WT cells treated with U18666A (WT + U18) were collected from top to bottom, separated by gel electrophoresis, and immunoblotted for Stx6, VAMP3, Rab11, Rab7, and Golgin-97 as indicated. Fractions 6–8 enriched with RE markers are highlighted.

(B) Quantification of total cholesterol in subcellular fractions isolated from CHO-WT, CHO M12, CHO 2-2, and U18666A-treated (CHO + U18666A) as shown in (A). (C) Isolated Golgi fractions and total cell lysates from CHO-WT (WT), CHO M12, CHO 2-2, and U18666A (U18)-treated CHO-WT cells were analyzed for Stx6 and GM130 as indicated.

(D and E) Quantification of Golgi-associated Stx6 and cholesterol, respectively.

mutant fibroblasts, as distribution of Golgi markers GM130, giantin (Figures S2A–S2D), or TGN46 (see Figure 1A) was comparable to controls. In addition, labeling of Stx6 interaction partners VAMP4 (see Figure 5A) or Stx16 was similar in CHO-M12 and CHO 2-2 cells compared to CHO-WT cells (not shown). Electron microscopy confirmed normal Golgi morphology in NPC1 mutant cells at the ultrastructural level (Figures S2E and S2F).

Although Stx6 has also been identified in EE (Simonsen et al., 1999), very little colocalization was observed between Stx6 and EEA1 (EE) (~10%), Rab4-GFP (early RE), or with Rab7 or Rab9 (LE markers) in CHO-WT cells (data not shown). However, Stx6 peripheral cytoplasmic vesicular structures clearly colocalized with the RE marker VAMP3 in CHO M12, CHO 2-2, and U18666A-treated CHO-WT cells (insets in Figure 2A; quantification of Stx6/VAMP3 in Figure 2B). In addition, in CHO-NPC1

mutants and in U18666A-treated CHO-WT, Stx6 was also present in the PNRE and partially colocalized with transferrin-tetramethylrhodamine isothiocyanate (Tf-TRITC), endogenous Rab11 (Figure S3), and transferrin receptor (TfR; data not shown). Therefore, cholesterol depletion in the TGN is associated with Stx6 translocation to two distinctive RE structures: the PNRE (positive for Rab11 and internalized transferrin) and peripheral, small vesicular VAMP3 structures.

In support of this, increased colocalization of Stx6 with Tf-fluorescein isothiocyanate (FITC), indicative of the recycling compartment, was evident in NPC1 mutant fibroblasts (GM03123 and G1) as well as U18666A-treated HSF (Figure 2C; quantification in Figure 2D).

To corroborate the immunofluorescence data, subcellular fractionation was performed in CHO-WT, CHO M12, CHO 2-2, and CHO-WT cells treated with U18666A (Figure 3A). Consistent

**Figure 2. Translocation of Stx6 into RE in NPC1 Mutant Cells**

(A) CHO-WT, CHO M12, CHO 2-2, and U18666A-treated CHO-WT cells were immunolabeled with anti-Stx6 (green) and anti-VAMP3 (red). Enlarged areas show regions of interest. Arrowheads (insets) indicate colocalization of Stx6 with VAMP3, and arrows indicate Stx6 localization in PNRE of NPC1 mutant cell lines CHO M12, CHO 2-2, and U18666A-treated CHO-WT, but not in CHO-WT control cells. The scale bars represent 10 and 2  $\mu$ m.

(B) Stx6/VAMP3 colocalization was quantified as described in Figure 1.

(C) Colocalization of Stx6 with Tf-TRITC in HSF, U18666A-treated HSF, and G03123 and G1 fibroblasts. To label the recycling compartment, cells were allowed to internalize Tf-TRITC (red) for 1 hr, fixed, and immunostained for Stx6 (green). Square areas (insets) show regions of interest. The scale bars represent 20 and 2  $\mu$ m.

(D) Quantification of Stx6/Tf-TRITC colocalization.

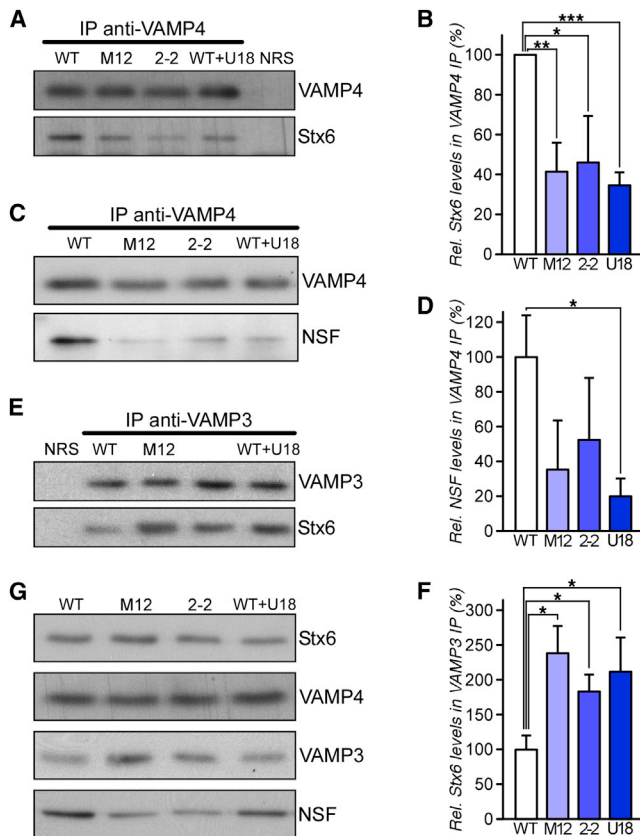


**Figure 4. Characterization of Stx6-Containing SNARE Complexes in NPC Mutant CHO Cells**

(A) Cell lysates from CHO-WT (WT), CHO M12, CHO 2-2, and U18666A-treated CHO-WT (WT + U18) cells were immunoprecipitated with anti-VAMP4 or control antibody (normal rabbit serum [NRS]) and analyzed for coimmunoprecipitation of Stx6. IP, immunoprecipitate.  
 (B) Quantification in percentage of (A).  
 (C) Immunoprecipitation of VAMP4 and coimmunoprecipitation of NSF is shown as indicated.  
 (D) Quantification of (C).  
 (E) Characterization of Stx6-containing VAMP3 immunoprecipitates from RE-enriched subcellular fractions (see nos. 6–8 in Figure 3A) from CHO-WT, CHO M12, CHO 2-2, and U18666A-treated CHO-WT.  
 (F) Quantification of (E).  
 (G) Total Stx6, VAMP4, VAMP3, and NSF levels in cell lysates from CHO-WT, CHO M12, CHO 2-2, and CHO-WT treated with U18666A (WT + U18).

with the microscopy, in CHO-WT cells, Stx6 appears mostly in the heavy fractions of the gradient (nos. 10–13), together with TGN (Golgin-97) and plasma membrane ( $\text{Na}^+\text{K}^+\text{-ATPase}$ ; not shown) markers. However, in all NPC1 mutant models, Stx6 accumulated in fractions 7–9, which were highly enriched with RE markers (Rab11 and VAMP3 in nos. 6–8) (Figure 3A). Hence, although subcellular fractionation methods have limited ability to separate TGN and RE in CHO cells (Hao et al., 2002), these findings correlate with the translocation of Stx6 into RE of NPC mutant cells observed by immunofluorescence microscopy.

The distribution of cholesterol along the sucrose gradient was in agreement with published data. In CHO-WT cells, cholesterol

was elevated in heavy fractions containing plasma membrane and Golgi membranes (nos. 10–13). In contrast, NPC1 mutant CHO cell lines showed a diminution of cholesterol in the plasma membrane and Golgi fractions, whereas cholesterol levels were elevated in Rab7-positive LE and Rab11/VAMP3-positive RE fractions (Figure 3B). In line with these findings, a significant reduction of cholesterol and Stx6 in isolated Golgi fractions from CHO M12, CHO 2-2, and CHO-WT cells treated with U18666A was observed (Figures 3C–3E).

### Cholesterol Distribution at the TGN-RE Interface Determines Stx6/VAMP4 and Stx6/VAMP3 SNARE Complex Formation

Stx6 associates with various SNAREs at multiple locations in endo- and exocytic pathways (Murray et al., 2005; Wendler and Tooze, 2001). Because Stx6 accumulated in RE upon diminution of cholesterol in the Golgi, we investigated if this could be linked to possible alterations of SNARE complex formation in post-Golgi and retrograde transport pathways. We particularly focused on the v-SNAREs VAMP3 and VAMP4, both recognized partners of Stx6 at the TGN-endosome interface (Ganley et al., 2008; Mallard et al., 2002; Tran et al., 2007) and involved in integrin recycling (Riggs et al., 2012; Skalski et al., 2010) (see next section).

VAMP4 is a v-SNARE protein with a TGN retention domain (Zeng et al., 2003), cycling from the cell surface to the TGN via sorting endosomes and RE (Tran et al., 2007) to complex with t-SNAREs Stx6/Stx16/Vti1a in the TGN. We hypothesized that NPC1-mutant-induced reduction of cholesterol and Stx6 in the TGN (Figures 1, 2, and 3) could modify VAMP4/Stx6 complex formation.

Indeed, coimmunoprecipitation of Stx6 and VAMP4 was significantly decreased in CHO M12, CHO 2-2, and U18666A-treated CHO-WT cells compared to controls (Figure 4A; see quantification in Figure 4B). Total amounts of Stx6 and VAMP4 were comparable in all cell lines (Figure 4G). Decreased colocalization of VAMP4 and Stx6 in CHO-NPC1 mutant cells support these findings (Figure 5A). VAMP4 overexpression in NPC mutant models did not restore Stx6 localization at the TGN (data not shown). In all NPC1-mutant-like models, decreased VAMP4/Stx6 interaction was associated with low *N*-ethylmaleimide-sensitive factor (NSF) levels in the immunoprecipitates, suggesting less functional VAMP4/Stx6 complexes in the Golgi (Figures 4C and 4F).

Moreover, the increased colocalization of Stx6 with RE markers (Figures 2A and 2B) was associated with a significantly increased amount of VAMP3/Stx6 immunocomplexes when a pool of RE-enriched membrane fractions (see fractions 6–8 in Figure 3A) was used for immunoprecipitation with anti-VAMP3 (Figures 4E and 4F).

### Modulation of Various Cholesterol Pools Differentially Regulate Stx6 Localization

As further proof of concept, in CHO-WT cells, expression of loss-of-function NPC1 mutant P692S, which cannot bind cholesterol and inhibits LE-chol export (Du et al., 2011; Millard et al., 2005; Ohgami et al., 2004), led to Stx6 accumulation in vesicular structures. On the contrary, in CHO M12 and CHO 2-2 cells, the

ectopic expression of wild-type NPC1 restored cellular cholesterol distribution and rescued the prominent steady state of Stx6 in the TGN (85% in CHO M12 and 65% in CHO 2-2 cells) (Figure S4).

Trafficking of cholesterol derived from LDLs or high-density lipoproteins (HDLs) follows different intracellular routes. Whereas internalized LDL cholesterol can be found in the Golgi at later time points (Garver et al., 2002), even in NPC1 mutant cells (Coxey et al., 1993), HDL-derived cholesterol rapidly enters the recycling compartment (Heeren et al., 2001, 2004; Röhrli et al., 2012). Therefore, we addressed if loading with LDL cholesterol could abrogate Stx6 mislocation into RE in NPC mutant cells. Indeed, loading CHO M12 and CHO 2-2 with LDL for 24 hr re-established the steady-state Stx6 TGN staining pattern (>88%) (Figure 5A). In contrast, incubation of CHO-WT cells with HDL for 30 min resulted in a Stx6 distribution reminiscent of the NPC1 phenotype, with Stx6 being much more dispersed in punctate structures and associated with diminished VAMP4 colocalization (Figure 5B; quantification of colocalization between Stx6 and VAMP4  $\pm$  LDL/HDL is given).

To address if the lipidic microdomain organization of TGN membranes could trigger Stx6 translocation, CHO-WT cells were treated with D-ceramide-C6, known to interfere with sphingomyelin (SM) levels and formation of SM-rich domains in Golgi membranes (Duran et al., 2012). However, Stx6 location remained unchanged after 30 or 60 min treatment with D-ceramide-C6 (Figure S5), further implicating cholesterol levels in RE and/or TGN being responsible for Stx6 translocation.

To study if increased interaction of Stx6 with VAMP3 was responsible for the pronounced engagement of Stx6 in RE, NPC mutant cell lines were transfected with the catalytic light chain of tetanus neurotoxin (L-TeTx), which selectively cleaves and inhibits VAMP3 (McMahon et al., 1993). Yet, upon L-TeTx overexpression and concomitant VAMP3 inhibition, Stx6 remained partially scattered (Figure 5C) and still colocalized with TfR in the recycling compartment of CHO M12, CHO 2-2, and U18666A-treated CHO-WT cells (data not shown).

All together, our data support the hypothesis that cholesterol levels in Golgi and RE membranes fine-tune Stx6 localization and Stx6/VAMP4/VAMP3 complex formation at the TGN/endo-some interface.

### Stx6 Accumulation in RE Inhibits Integrin Recycling

To examine the potential functional consequences of cholesterol imbalance causing Stx6 mislocation, we determined trafficking of integrins (Riggs et al., 2012; Tiwari et al., 2011). Integrins consist of  $\alpha$  and  $\beta$  subunits that bind ECM proteins to regulate cell adhesion and migration (Caswell and Norman, 2008). Integrins undergo endo-/exocytic transport, and surface integrin recycling regulates cell migration (Caswell and Norman, 2006; Caswell et al., 2009; Muller et al., 2009). Importantly, recycling of the FN receptor integrins  $\alpha$ V $\beta$ 3 and  $\alpha$ 5 $\beta$ 1 is regulated by Stx6 in several cellular models (Riggs et al., 2012; Tiwari et al., 2011; Zhang et al., 2008).

RNAi knockdown experiments confirmed that Stx6 regulates integrin localization in CHO cells. Whereas Stx6 depletion in CHO-WT significantly reduced  $\alpha$ V and  $\alpha$ 5 integrin cell-surface expression (65%  $\pm$  5% and 20%  $\pm$  2.2%, respectively) (Fig-

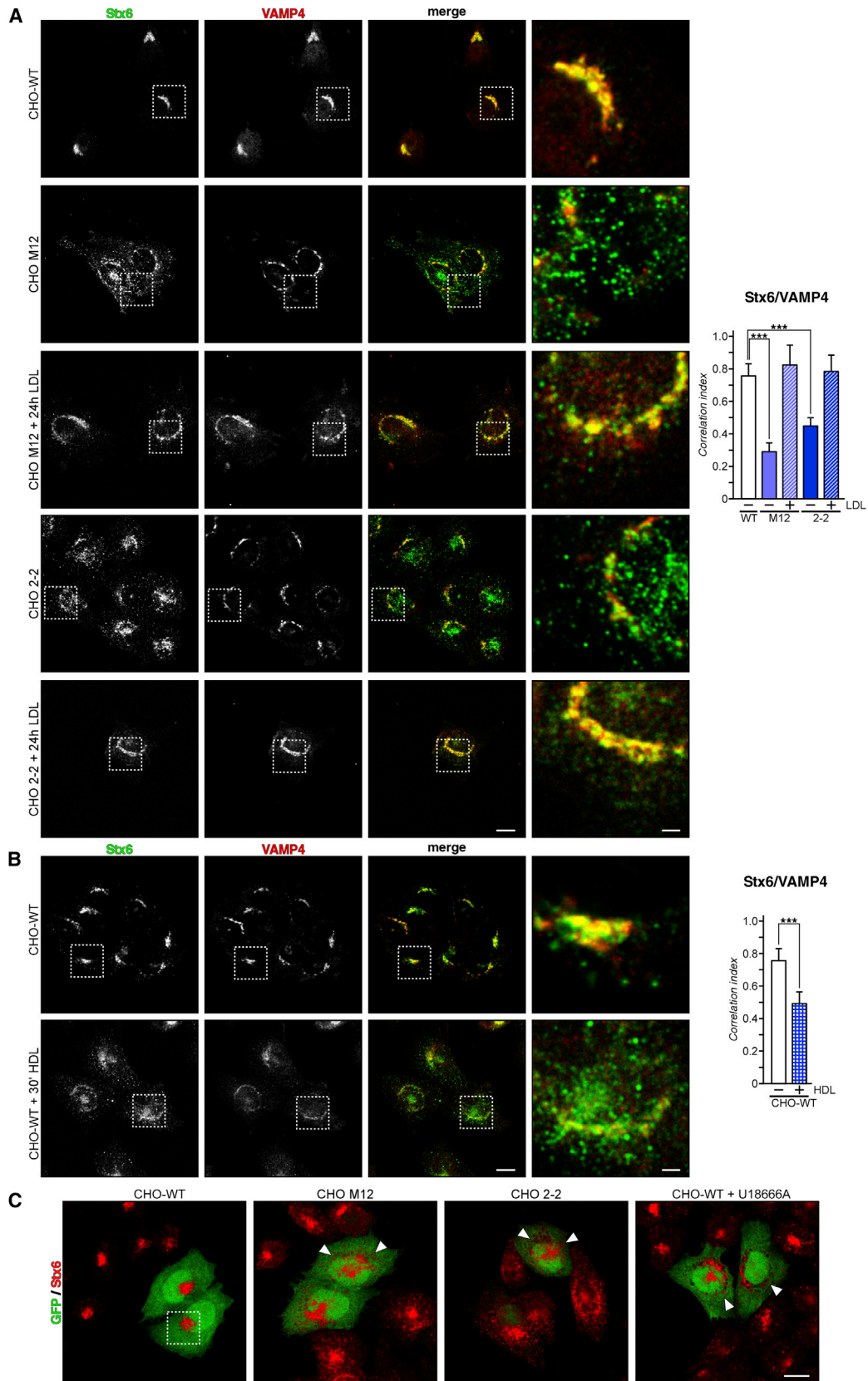
ure S6A, compare lanes 3 and 4), Stx4 depletion (50%  $\pm$  8%) did not alter  $\alpha$ V and  $\alpha$ 5 integrin cell-surface localization (Figures S6A and S6B, compare lanes 2 and 4). Flow cytometry to compare cell-surface expression of integrins in control CHO-WT, NPC1 mutant cells (CHO M12 and CHO 2-2), and CHO-WT treated with U18666A showed a significant reduction in cell surface  $\alpha$ V,  $\alpha$ 5, and  $\beta$ 3 integrins in all NPC1 mutant models compared to controls (35% for  $\alpha$ V and 25% for  $\alpha$ 5 and  $\beta$ 3 in CHO; Figure 6A).

In support of these data, cell microscopy identified  $\alpha$ 5 integrin mainly at the plasma membrane in CHO-WT (Figure 6B) but increasingly in TfR- or endogenous Rab11-positive (data not shown) perinuclear structures in CHO M12, CHO 2-2, and U18666A-treated CHO-WT (Figure 6B). Thus, upon decreased cholesterol levels in the Golgi,  $\alpha$ 5,  $\beta$ 1, and possibly other integrins accumulate in the PNRE (see squares in Figure 6B).

To substantiate these findings,  $\alpha$ V integrin recycling in control and NPC1 mutant CHO cells was compared. Cell-surface proteins, including  $\alpha$ V integrins, were biotinylated (Figure 6C, lanes 1 and 5) and then internalized for 30 min. Residual surface biotin was removed (Figure 6C, lanes 2 and 6), and cells were allowed to recycle the internal pool of biotinylated proteins for 30 min (lanes 3 and 7). After removal of recycled plasma membrane biotin, the remaining pool of nonrecycled internal  $\alpha$ V integrins could be detected (lanes 4 and 8) (Roberts et al., 2001; Veale et al., 2010). Almost all  $\alpha$ V integrins were recycled in controls (lane 4), whereas approximately 10%–20% of biotinylated  $\alpha$ V integrins remained in RE in CHO M12, CHO 2-2, and U18666A-treated CHO-WT cells (Figure 6D; quantification). Hence, diminution of TGN cholesterol in NPC1 mutant CHO cells interferes with  $\alpha$ V integrin recycling.

Further validating that lowering cholesterol levels in the Golgi interfered with integrin recycling, NPC1-P692S-GFP expression in CHO-WT cells strongly reduced cell-surface levels of  $\alpha$ V,  $\alpha$ 5, and  $\beta$ 3 integrins as judged by flow cytometry (Figure S6C). Moreover, in CHO M12 and CHO 2-2, wild-type NPC1 robustly reduced the perinuclear accumulation of  $\alpha$ 5 integrin, which corresponds to the RE compartment (Figure S6D), further reinforcing the involvement of LE-chol for integrin cell-surface expression.

To provide physiological relevance of the data sets derived from cellular and pharmacological rodent NPC1 mutant models, integrin and Stx6 localization in human NPC1 mutant fibroblasts were analyzed. In agreement with the results obtained from NPC1 mutant CHO models, cell-surface expression of  $\alpha$ V,  $\alpha$ 5, and  $\beta$ 3 integrins in GM03123 and G1 fibroblasts was reduced (~50% for  $\alpha$ V and ~40% for  $\alpha$ 5 and  $\beta$ 3 integrins; Figure 6E).  $\alpha$ 5 $\beta$ 1 integrins were located on the cell surface of HSF control fibroblasts but accumulated in intracellular, VAMP3-containing RE structures of GM03123, G1, and U18666A-treated HSF (Figure 6F). It should be noted that the RE compartment is more dispersed in HSF and NPC1 mutant fibroblasts compared to CHO cells (Choudhury et al., 2004). As shown for the rodent NPC1 mutant models, profound integrin (and Stx6) accumulation in vesicular RE structures was not associated with altered Golgi morphology in GM03123, G1, or U18666A-treated HSF fibroblasts (Figures S2C, S2D, and S2F).



(legend on next page)

### Cholesterol Imbalance Inhibits Cell Migration

To address the impact of cholesterol-mediated Stx6 translocation into RE and the concomitant inhibition of integrin recycling on cell migration, scratch-wound-healing assays were performed in NPC1 mutant CHO cell models. Whereas control cells efficiently migrated into scratched areas, all NPC1 mutant-like models displayed a significantly reduced (40%–60%) capacity to migrate (Figure 7A). Using time-lapse video microscopy, individual cell mobility was examined. All NPC1 mutant CHO models as well as U18666A-treated CHO-WT cells showed a considerably lower cell velocity compared to controls (~30% for CHO; Figure 7B). Further supporting a role for Stx6 in regulating integrin recycling and cell migration, small interfering RNA (siRNA)-mediated depletion of Stx6 dramatically reduced cell migration in live-cell imaging studies and strongly reduced velocity in CHO-WT cells (~60%) (Figure 7C). Closer examination showed that, 2 hr postseeding, cell spreading was also significantly reduced in all NPC1 mutant cells (Figure 7D). Cell spread of CHO-WT and all NPC1 mutant models 12 hr after seeding was similar and consistent with other studies (Skalski and Copolino, 2005), excluding cellular dimensions as a potential inducer of reduced spreading in NPC1 mutants or upon drug treatment.

Next, we looked at the potential correlation of Stx6 engagement in RE with cell invasion. Using transwell migration and Matrigel invasion chambers, large numbers of control CHO-WT cells were observed migrating/invasive into the wells. In contrast, CHO M12 and CHO 2-2 cells displayed significantly reduced migratory/invasive capacity compared to controls (Figure 7E). We then compared the invasiveness of CHO-WT, CHO M12, and CHO 2-2 cells in *in vivo*-like settings using three-dimensional organotypic matrices that more closely recapitulate a tumor stromal environment (Timpson et al., 2011a, 2011b). CHO-WT cells moved into organotypic matrices in considerable numbers over a 21-day period. By contrast, and after normalization to cell number, invasion of CHO M12 and CHO 2-2 cells was significantly reduced by 50% ± 3% (Figure 7F). Finally, we compared cell migration in HSF from controls and NPC1 patients GM03123 and G1 (Choudhury et al., 2004; Rodríguez-Pascau et al., 2012). Supporting the data from rodent NPC1 mutant models, cell migration (~40%–60%), velocity (~20%), and cell spreading (~30%) were significantly reduced in GM03123 and G1 fibroblasts and U18666A-treated HSF, compared to controls (Figures 7G–7I). Taken together, diminution of cholesterol in the Golgi leads to a significant reduction in cell spreading, migration, and invasiveness of cells.

### DISCUSSION

The present study demonstrates that blockage of LE-chol export due to NPC1 mutation or U18666A treatment, and the concomitant imbalance of cholesterol in the TGN/endosomal boundaries, induces the accumulation of Stx6 in RE. This is associated with significant alterations in Stx6/VAMP3 and Stx6/VAMP4 SNARE complex formation, correlating with inhibition of integrin recycling and the diminution of cell-surface integrin expression to ultimately impair fundamental aspects of cell motility, possibly in a Stx6-dependent manner, as evidenced by reduced cell spreading, migration, and invasion in both two- and three-dimensional environmental context.

Data presented here suggest that the trafficking route of Stx6 between TGN and RE compartments and compartment-specific interaction of Stx6 with v-SNARES VAMP3 and VAMP4 are controlled through an ability of Stx6 to sense cholesterol levels in the TGN and RE. NPC1-mediated diminution of cholesterol in TGN membranes seems to trigger trafficking of Stx6 into cholesterol-enriched RE. Alternatively, elevated RE cholesterol could promote Stx6 translocation and increase the ability of Stx6 to interact with VAMP3. In fact, RE is the main intracellular cholesterol repository compartment of CHO cells, nonpolarized hepatoma HepG2 cells, fibroblasts (Maxfield and McGraw, 2004), and human B lymphocytes (Möbius et al., 2003). Indeed, selectively raising the RE cholesterol content with HDL increased Stx6 localization in RE.

Mechanistically, Stx6 may directly bind cholesterol as proposed recently (Hulce et al., 2013) or, alternatively, may sense cholesterol-dependent changes in overall membrane organization. Interestingly, neither alterations in SM levels and SM containing liquid-ordered domains nor selective inhibition of VAMP3 or VAMP4 overexpression altered Stx6 localization, further suggesting that Stx6 rather senses the amount of cholesterol, but not its impact on intrinsic membrane organization or availability of interacting partners. Strikingly, other proteins trafficking through TGN and endosomal compartments such as M6PR, TfR, and TGN46, or SNARE proteins such as Stx16, VAMP3, VAMP4, or Vti1a did not show cholesterol-sensitive alterations in cellular localization.

Although other alternative pathways may exist, our findings support a model that links cholesterol-sensitive SNARE proteins with final steps in integrin recycling (Day et al., 2011; Lang, 2007; Figure S7). Several studies associate Stx6 localization and function with the role of specialized cholesterol-rich microdomains and focal adhesion sites for integrin recycling, FAK signaling, and directional migration toward FN (Tiwari et al., 2011). Furthermore, Stx6 overexpression increases cell migration and is elevated in breast, liver, and prostate cancers (Riggs et al.,

#### Figure 5. LDL Loading Modulates Stx6 Localization in NPC1 Mutant CHO Cells

- (A) CHO-WT, CHO M12, and CHO 2-2 cells were incubated ± LDL (0.05 mg/ml) for 24 hr as indicated. Cells were fixed and immunolabeled with anti-Stx6 (green) and anti-VAMP4 (red); squares show perinuclear Golgi compacted labeling.
- (B) CHO-WT cells were incubated ± HDL (0.1 mg/ml) for 30 min, fixed, and labeled with anti-Stx6 and anti-VAMP4 as in (A). Control cells show compact Golgi Stx6/VAMP4 labeling. Cells treated with HDL show partially scattered Stx6 staining. The scale bars represent 10 and 2 μm (insets). Quantification as described in Figures 1 and 2.
- (C) CHO cells were transfected with pRES2-L-TeTx for 48 hr (green) and then fixed and stained with anti-Stx6 (red). Arrowheads point at disperse Stx6 structures in NPC1 mutant cells. The scale bar represents 10 μm.

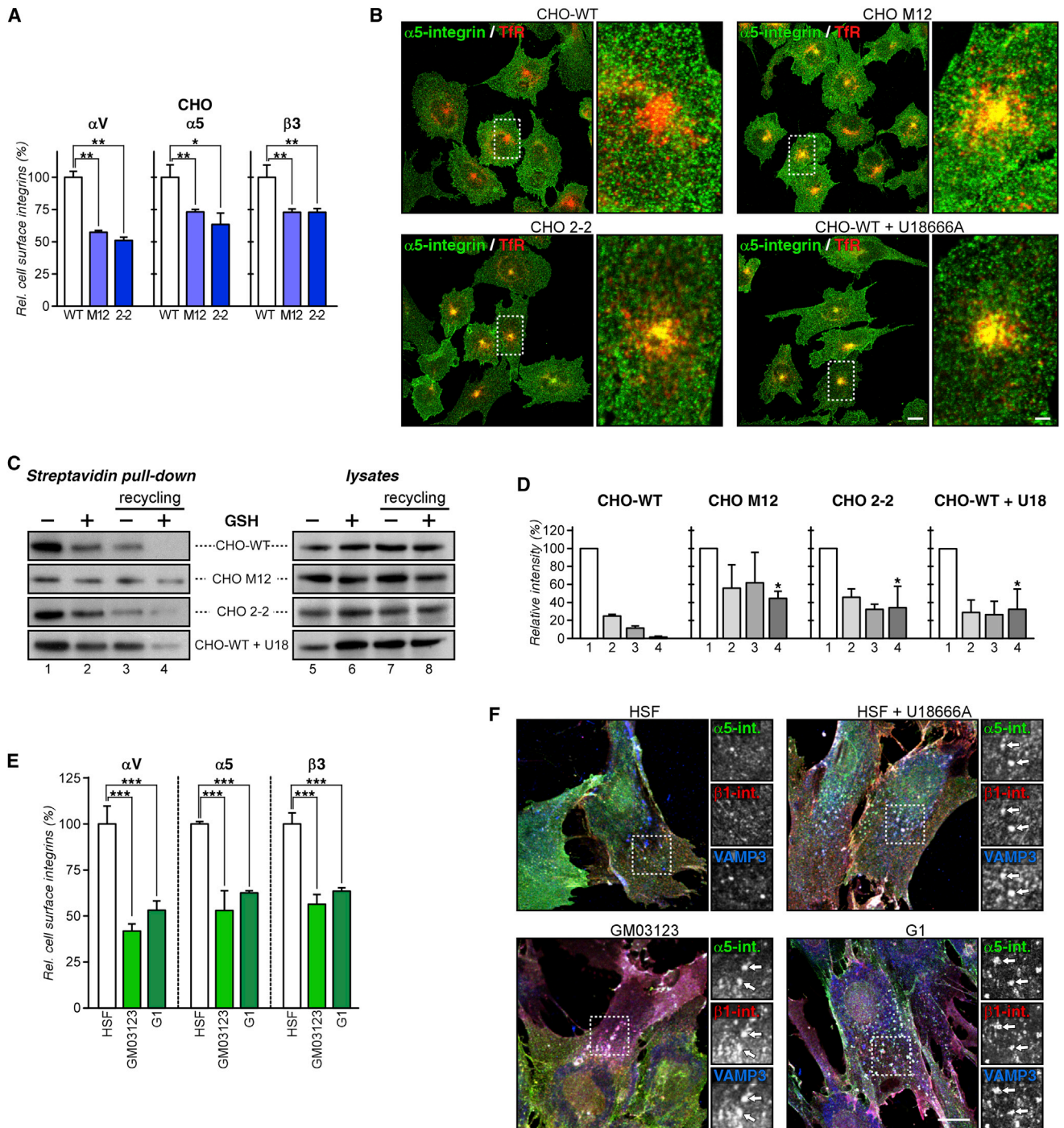


**Figure 6. Reduced Cell-Surface Expression of Integrins in NPC1 Mutant Cells**

(A) Cell-surface expression of  $\alpha V$ ,  $\alpha 5$ , and  $\beta 3$  integrins in CHO-WT, CHO M12, and CHO 2-2 cells plated onto FN was determined by flow cytometry. Values were normalized to CHO-WT.

(B) Colocalization of  $\alpha 5$  integrin (green) with TfR (red) in CHO-WT, CHO M12, CHO 2-2, and U18666A-treated CHO-WT cells. Squares highlight the RE at the perinuclear region, where  $\alpha 5$  integrin colocalizes with TfR in NPC mutant cells and U18666A-treated CHO-WT cells. The scale bars represent 10  $\mu m$  and 2  $\mu m$  (insets).

(C) Cell-surface biotinylated (streptavidin pull-down) and total (lysates)  $\alpha V$  integrin from CHO-WT, CHO M12, CHO 2-2, and U18666A-treated CHO-WT cells (glutathione [GSH], reduced L-glutathione) were analyzed by western blotting and quantified in (D).

(D) The relative amount of biotin-labeled  $\alpha V$  integrin at the cell surface (lanes 1 and 5), internalized after 30 min (lanes 2 and 6), total internalized recycled (lanes 3 and 7), and recycled (lanes 4 and 8) were quantified ( $n = 2$ ).

(legend continued on next page)

2012). Earlier work implicated cholesterol in the formation of signaling complexes containing  $\alpha$ V $\beta$ 3, CD47, and G proteins (Green et al., 1999) and control of cell adhesion and migration onto FN (Ramprasad et al., 2007). This possibly requires Rab11, which modulates cholesterol transport and homeostasis (Hölttä-Vuori et al., 2002) and facilitates the recycling of  $\beta$ 1 integrin (Powelka et al., 2004). Recent reports showing increased cholesterol requirements for breast cancer and A431 cell invasion (Freed-Pastor et al., 2012) and impaired A431 invasion upon inhibition of integrin recycling (Muller et al., 2009) support this model.

Delivery of LE-cholesterol is critical for cholesterol homeostasis in the endoplasmic reticulum and maintaining cholesterol levels in other compartments. NPC1 affects cholesterol delivery to the plasma membrane, and a substantial amount of LE-cholesterol being transported via NPC1 appears to traffic through Golgi membranes en route to the plasma membrane in human fibroblasts (Urano et al., 2008). However, cell-specific intracellular differences in cholesterol routes seem to exist, as BODIPY cholesterol did not label the Golgi apparatus in A431 cells (Kanerva et al., 2013).

Interestingly, as shown here and previously, prolonged LDL treatment in NPC1 mutant cells still delivered cholesterol to other compartments, including the Golgi, indicating alternative LDL cholesterol trafficking routes or incomplete blockage of cholesterol egress from LE in NPC1 mutant cells. In fact, in NPC1-deficient fibroblasts, cholesterol accumulates in *trans*-Golgi cisternae with the TGN remaining relatively cholesterol-deficient (Garver et al., 2002).

The pathways that deliver and control cholesterol levels in the RE are poorly understood. Major routes likely involve non-vesicular and vesicular trafficking from and to the plasma membrane (Mesmin and Maxfield, 2009). Although current fractionation methods to purify RE have limitations (Hao et al., 2002), cholesterol levels in Rab11/VAMP3-enriched fractions (fractions Nos. 7 and 8) were slightly elevated in NPC1 mutant cell models. Actually, prolonged LDL cholesterol loading, known to reach the Golgi, abrogated Stx6 localization in RE of NPC1 mutant models, indicating that cholesterol levels in the Golgi, and probably not in the RE, determine Stx6 localization. Also, addition of exogenous cholesterol to elevate plasma membrane and RE cholesterol did not alter Stx6 location at the TGN (not shown). Intriguingly, methyl- $\beta$ -cyclodextrin mediated cholesterol depletion at the plasma membrane accentuated Stx6 accumulation in RE (not shown). As removal of cell-surface cholesterol induces translocation of SNAP23 and Stx4 from the plasma membrane to the Golgi (Reverter et al., 2011), the possibility of SNAP23/VAMP4 association in this compartment cannot be excluded, perhaps competing with Stx6/VAMP4 assembly (Skalski et al., 2010).

Beyond the scope of this study, other mechanisms include oxysterol-binding protein (OSBP) and OSBP-related proteins, which have been implicated in the distribution of sterols among

intracellular organelles. OSBP regulates levels of PI(4)P, ceramide, but also cholesterol in the Golgi (Duran et al., 2012) and is essential for the localization of intra-Golgi v-SNAREs GS28 and GS15 (Nishimura et al., 2013).

Utilizing VAMP3-targeting neurotoxins (L-TeTx) or RNAi knockdown approaches (Luftman et al., 2009; Proux-Gillardeaux et al., 2005; Skalski and Coppolino, 2005), VAMP3 has been shown to be essential for cell migration, spreading, and integrin-dependent cell adhesion. However, as shown here and by others (Zylbersztejn and Galli, 2011), other SNAREs as well as additional modulators, such as cholesterol, also contribute to regulate integrin-trafficking pathways and, consequently, cell migration.

Up to date, only two studies have analyzed and linked trafficking (and function) of Stx6 with the recycling of integrins and cell migration (Riggs et al., 2012; Tiwari et al., 2011). However, these studies did not reveal a possible role for cholesterol in the regulation of Stx6 location and function. In line with data shown here, both studies showed that Stx6 loss of function interfered with integrin trafficking: diminution of cell-surface integrin or increased ubiquitination of integrins and diversion into the degradation pathway (Riggs et al., 2012; Tiwari et al., 2011). In HeLa cells, Stx6 at the TGN was required for the trafficking of  $\alpha$ 3 $\beta$ 1 integrins (Riggs et al., 2012). In endothelial cells, Stx6 may play a role in the maintenance of lipid or protein composition and/or domain organization of Rab GTPases on the endosome membrane, thereby facilitating sorting from EE (Tiwari et al., 2011).

Although our results do not completely identify cholesterol-imbalance-triggered Stx6 mislocalization as the sole cause of inhibited integrin recycling, data presented here strongly indicate that both a diminution of cholesterol in TGN membranes, caused by NPC1 loss of function, or alternatively increasing cholesterol levels in recycling endosomes, e.g., by exposure to HDL, triggers Stx6 accumulation in RE, which is associated with increased association with VAMP3 and Rab11. Therefore, similar to the postulated role of VAMP3 in RE (Proux-Gillardeaux et al., 2005; Tayeb et al., 2005), Stx6 in the TGN may be necessary to ensure accurate dynamics of integrin recycling. Importantly, this study suggests that the levels of cholesterol in these trafficking compartments ultimately contribute to control mechanisms that regulate the recycling of integrins. Hence, this study identifies a regulatory circuit of cholesterol-sensitive SNARE interactions that potentially drive integrin-dependent cell migration and invasion.

Lipid storage disorders associated with NPC1/NPC2 mutations manifest in neurological disorders, hepato- and/or splenomegaly, and cardiovascular complications. Remarkably, NPC1-dependent cholesterol availability has now also been identified critical for proper cell movement in early zebrafish morphogenesis (Schwend et al., 2011). This regulatory role of NPC1 identifies a link between a cholesterol-sensitive member of the SNARE family, which eventually may affect integrin

(E) Cell-surface expression of  $\alpha$ V,  $\alpha$ 5, and  $\beta$ 3 integrins in HSF, G03123, and G1 fibroblasts plated onto FN was determined by flow cytometry. Values were normalized to HSF.

(F) Colocalization of VAMP3 (blue) with  $\alpha$ 5 (green) and  $\beta$ 1 integrins (red) in HSF, U18666A-treated HSF, G03123, and G1 fibroblasts (colocalization of VAMP3 with  $\alpha$ 5 and  $\beta$ 1 integrins is indicated by small white arrows). The scale bar represents 20  $\mu$ m.

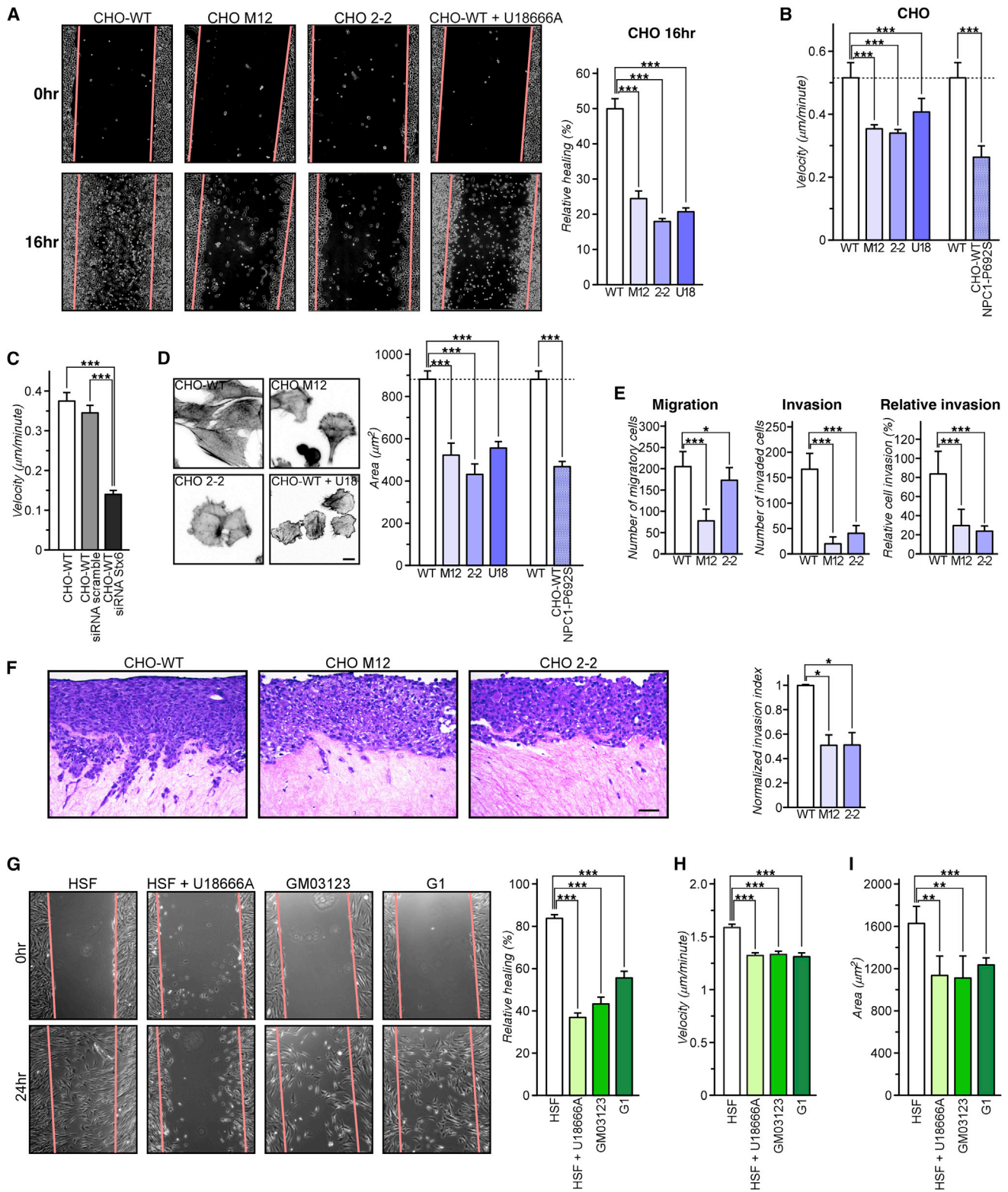


**Figure 7. Reduced Cell Migration and Invasion in CHO and HSF NPC1 Mutant Cells**

(A) Wound closure of CHO-WT, CHO M12, CHO 2-2, and U18666A-treated CHO-WT cells after 16 hr was calculated and is given as relative healing (%). Data represent the mean  $\pm$  SEM from three independent experiments done in triplicate. Representative images of CHO-WT, CHO M12, CHO 2-2, and U18666A-treated CHO-WT are shown.

(legend continued on next page)

trafficking to regulate cell-surface integrin expression and, consequently, cell migration.

## EXPERIMENTAL PROCEDURES

Details of Experimental Procedures can be found in the [Supplemental Experimental Procedures](#).

### Reagents and Antibodies

For a complete list of reagents, antibodies ([Table S1](#)), and more detailed information on cell culture, transfections, cholesterol measurements, U18666A treatment, immunoprecipitations, statistics, and subcellular fractionation, see the [Supplemental Experimental Procedures](#).

### Microscopic Techniques and Image Analysis

The preparation of cells for immunofluorescence and the acquisition and quantification of images is explained in detail in the [Supplemental Experimental Procedures](#).

### Flow Cytometry

Cells were harvested in PBS and 0.5 mM EDTA, resuspended in ice-cold PBS, 1% fetal calf serum (fluorescence-activated cell sorting [FACS] buffer), and incubated in FACS buffer with anti-integrins (0.01  $\mu\text{g/ml}$   $\alpha 5$  and  $\beta 3$ ; 0.02  $\mu\text{g/ml}$   $\alpha V$ ) for 1 hr at 4°C. Cells were washed, incubated with fluorescently tagged secondary antibody for 1 hr, and then washed. Cell-surface fluorescence was measured using a BD FACS Cantoll cytometer.

### Analysis of Cell Migration

Spreading, organotypic invasion, and Matrigel migration/invasion assays are explained in detail in the [Supplemental Experimental Procedures](#).

## SUPPLEMENTAL INFORMATION

Supplemental information includes Supplemental Experimental Procedures, seven figures, and one table and can be found with this article online at <http://dx.doi.org/10.1016/j.celrep.2014.03.043>.

## ACKNOWLEDGMENTS

This study was supported by grants BFU2012-36272 and CSD2009-00016 from Ministerio de Economía y Competitividad (MEC) and PI042182 from Fundació Marató TV3 (Spain) to C.E. T.G. is supported by the National Health and Medical Research Council of Australia (NHMRC; 510294) and the University of Sydney (2010-02681). R.Z.M. acknowledges support through the NHMRC Fellowship (457247). P.T. acknowledges support from the NHMRC, Australian Research Council, and Cancer Institute New South Wales (CINSW). We are thankful to M. Calvo, N. Cortadellas, and A. García (Centres Científics i

Tecnològics, Universitat de Barcelona) for their help in confocal and electron microscopy; M. Sawicka (Medical School of Silesia, Poland) and T. Nishizumi (University of Miyasaki, Japan) for help in the spreading assay; and M. Molinos and H. Gutierrez for technical assistance. M.R. and A.Á.G. are grateful to MEC for a short-term fellowship in Sydney, Australia at the University of Sydney and the University of New South Wales, respectively.

Received: June 18, 2013

Revised: December 30, 2013

Accepted: March 17, 2014

Published: April 17, 2014

## REFERENCES

- Blanchette-Mackie, E.J., Dwyer, N.K., Amende, L.M., Kruth, H.S., Butler, J.D., Sokol, J., Comly, M.E., Vanier, M.T., August, J.T., Brady, R.O., et al. (1988). Type-C Niemann-Pick disease: low density lipoprotein uptake is associated with premature cholesterol accumulation in the Golgi complex and excessive cholesterol storage in lysosomes. *Proc. Natl. Acad. Sci. USA* *85*, 8022–8026.
- Bock, J.B., Klumperman, J., Davanger, S., and Scheller, R.H. (1997). Syntaxin 6 functions in trans-Golgi network vesicle trafficking. *Mol. Biol. Cell* *8*, 1261–1271.
- Caswell, P.T., and Norman, J.C. (2006). Integrin trafficking and the control of cell migration. *Traffic* *7*, 14–21.
- Caswell, P., and Norman, J. (2008). Endocytic transport of integrins during cell migration and invasion. *Trends Cell Biol.* *18*, 257–263.
- Caswell, P.T., Vadrevu, S., and Norman, J.C. (2009). Integrins: masters and slaves of endocytic transport. *Nat. Rev. Mol. Cell Biol.* *10*, 843–853.
- Choudhury, A., Sharma, D.K., Marks, D.L., and Pagano, R.E. (2004). Elevated endosomal cholesterol levels in Niemann-Pick cells inhibit rab4 and perturb membrane recycling. *Mol. Biol. Cell* *15*, 4500–4511.
- Choudhury, A., Marks, D.L., Proctor, K.M., Gould, G.W., and Pagano, R.E. (2006). Regulation of caveolar endocytosis by syntaxin 6-dependent delivery of membrane components to the cell surface. *Nat. Cell Biol.* *8*, 317–328.
- Coxey, R.A., Pentchev, P.G., Campbell, G., and Blanchette-Mackie, E.J. (1993). Differential accumulation of cholesterol in Golgi compartments of normal and Niemann-Pick type C fibroblasts incubated with LDL: a cytochemical freeze-fracture study. *J. Lipid Res.* *34*, 1165–1176.
- Cubells, L., Vilà de Muga, S., Tebar, F., Wood, P., Evans, R., Ingelmo-Torres, M., Calvo, M., Gaus, K., Pol, A., Grewal, T., and Enrich, C. (2007). Annexin A6-induced alterations in cholesterol transport and caveolin export from the Golgi complex. *Traffic* *8*, 1568–1589.
- Cubells, L., Vilà de Muga, S., Tebar, F., Bonventre, J.V., Balsinde, J., Pol, A., Grewal, T., and Enrich, C. (2008). Annexin A6-induced inhibition of cytoplasmic phospholipase A2 is linked to caveolin-1 export from the Golgi. *J. Biol. Chem.* *283*, 10174–10183.

(B) Individual cell tracks of CHO-WT, CHO M12, CHO 2-2, U18666A-treated CHO-WT, and CHO-WT expressing NPC1-P692S, plated onto FN, and analyzed by time-lapse video microscopy for 12 hr. Individual cell tracks were generated, and the speed (velocity) was calculated.

(C) CHO-WT expressing siRNA-targeting Stx6 or scrambled were plated on FN, and individual cell tracks were analyzed by time-lapse video microscopy for 12 hr.

(D) Cell spreading areas were determined for CHO-WT, CHO M12, CHO 2-2, U18666A-treated CHO-WT, and NPC1-P692S-transfected CHO-WT cells 2 hr after seeding onto FN-coated plates. Areas of 100 cells per experiment were quantified. Representative fields of CHO cell lines are shown.

(E) Transwell migration and invasion of CHO-WT, CHO M12, and CHO 2-2 cells. Migrating and invading cells from six fields/cell line were quantified, and relative migration and invasion was calculated.

(F) Organotypic invasion assay with CHO-WT, CHO M12, and CHO 2-2 cells plated on three-dimensional matrices of rat-tail collagen I. Cells were allowed to invade for 21 days, fixed, and processed for hematoxylin and eosin staining. The invasion index was calculated as a ratio of the proportion of cells characterized by complete matrix envelopment, as opposed to those on the surface of the matrix. Representative images of three independent experiments are shown. The scale bar represents 50  $\mu\text{m}$ .

(G) Relative wound closure (healing) of HSF, U18666A-treated HSF, and G03123 and G1 fibroblasts after 24 hr was calculated. Data represent mean values  $\pm$  SEM from three independent experiments done in triplicate.

(H) Individual cell tracking of HSF, U18666A-treated HSF, and G03123 and G1 fibroblasts plated on FN was analyzed by time-lapse video microscopy for 12 hr. Velocity (speed) of individual cell migration tracks were quantified.

(I) Cell spreading area of HSF, U18666A-treated HSF, and G03123 and G1 fibroblasts, plated on FN, was determined 2 hr after seeding. One hundred cells per experiment were quantified.

- Dahl, N.K., Reed, K.L., Daunais, M.A., Faust, J.R., and Liscum, L. (1992). Isolation and characterization of Chinese hamster ovary cells defective in the intracellular metabolism of low density lipoprotein-derived cholesterol. *J. Biol. Chem.* **267**, 4889–4896.
- Day, P., Riggs, K.A., Hasan, N., Corbin, D., Humphrey, D., and Hu, C. (2011). Syntaxins 3 and 4 mediate vesicular trafficking of  $\alpha 5\beta 1$  and  $\alpha 3\beta 1$  integrins and cancer cell migration. *Int. J. Oncol.* **39**, 863–871.
- Dozynkiewicz, M.A., Jamieson, N.B., Macpherson, I., Grindlay, J., van den Berghe, P.V., von Thun, A., Morton, J.P., Gourley, C., Timpson, P., Nixon, C., et al. (2012). Rab25 and CLIC3 collaborate to promote integrin recycling from late endosomes/lysosomes and drive cancer progression. *Dev. Cell* **22**, 131–145.
- Du, X., Kumar, J., Ferguson, C., Schulz, T.A., Ong, Y.S., Hong, W., Prinz, W.A., Parton, R.G., Brown, A.J., and Yang, H. (2011). A role for oxysterol-binding protein-related protein 5 in endosomal cholesterol trafficking. *J. Cell Biol.* **192**, 121–135.
- Duran, J.M., Campelo, F., van Galen, J., Sachsenheimer, T., Sot, J., Egorov, M.V., Rentero, C., Enrich, C., Polishchuk, R.S., Goñi, F.M., et al. (2012). Sphingomyelin organization is required for vesicle biogenesis at the Golgi complex. *EMBO J.* **31**, 4535–4546.
- Freed-Pastor, W.A., Mizuno, H., Zhao, X., Langerød, A., Moon, S.H., Rodriguez-Barrueco, R., Barsotti, A., Chicas, A., Li, W., Polotskaia, A., et al. (2012). Mutant p53 disrupts mammary tissue architecture via the mevalonate pathway. *Cell* **148**, 244–258.
- Ganley, I.G., Espinosa, E., and Pfeffer, S.R. (2008). A syntaxin 10-SNARE complex distinguishes two distinct transport routes from endosomes to the trans-Golgi in human cells. *J. Cell Biol.* **180**, 159–172.
- Garver, W.S., Krishnan, K., Gallagos, J.R., Michikawa, M., Francis, G.A., and Heidenreich, R.A. (2002). Niemann-Pick C1 protein regulates cholesterol transport to the trans-Golgi network and plasma membrane caveolae. *J. Lipid Res.* **43**, 579–589.
- Green, J.M., Zhelesnyak, A., Chung, J., Lindberg, F.P., Sarfati, M., Frazier, W.A., and Brown, E.J. (1999). Role of cholesterol in formation and function of a signaling complex involving  $\alpha v\beta 3$ , integrin-associated protein (CD47), and heterotrimeric G proteins. *J. Cell Biol.* **146**, 673–682.
- Hao, M., Lin, S.X., Karylowski, O.J., Wüstner, D., McGraw, T.E., and Maxfield, F.R. (2002). Vesicular and non-vesicular sterol transport in living cells. The endocytic recycling compartment is a major sterol storage organelle. *J. Biol. Chem.* **277**, 609–617.
- Heeren, J., Grewal, T., Jäckle, S., and Beisiegel, U. (2001). Recycling of apolipoprotein E and lipoprotein lipase through endosomal compartments in vivo. *J. Biol. Chem.* **276**, 42333–42338.
- Heeren, J., Grewal, T., Laatsch, A., Becker, N., Rinninger, F., Rye, K.A., and Beisiegel, U. (2004). Impaired recycling of apolipoprotein E4 is associated with intracellular cholesterol accumulation. *J. Biol. Chem.* **279**, 55483–55492.
- Hölttä-Vuori, M., Tanhuanpää, K., Möbius, W., Somerharju, P., and Ikonen, E. (2002). Modulation of cellular cholesterol transport and homeostasis by Rab11. *Mol. Biol. Cell* **13**, 3107–3122.
- Hulce, J.J., Cognetta, A.B., Niphakis, M.J., Tully, S.E., and Cravatt, B.F. (2013). Proteome-wide mapping of cholesterol-interacting proteins in mammalian cells. *Nat. Methods* **10**, 259–264.
- Ikonen, E. (2006). Mechanisms for cellular cholesterol transport: defects and human disease. *Physiol. Rev.* **86**, 1237–1261.
- Ikonen, E. (2008). Cellular cholesterol trafficking and compartmentalization. *Nat. Rev. Mol. Cell Biol.* **9**, 125–138.
- Jones, M.C., Caswell, P.T., and Norman, J.C. (2006). Endocytic recycling pathways: emerging regulators of cell migration. *Curr. Opin. Cell Biol.* **18**, 549–557.
- Kanerva, K., Uronen, R.L., Blom, T., Li, S., Bittman, R., Lappalainen, P., Peränen, J., Raposo, G., and Ikonen, E. (2013). LDL cholesterol recycles to the plasma membrane via a Rab8a-Myosin5b-actin-dependent membrane transport route. *Dev. Cell* **27**, 249–262.
- Lang, T. (2007). SNARE proteins and ‘membrane rafts’. *J. Physiol.* **585**, 693–698.
- Lang, T., Bruns, D., Wenzel, D., Riedel, D., Holroyd, P., Thiele, C., and Jahn, R. (2001). SNAREs are concentrated in cholesterol-dependent clusters that define docking and fusion sites for exocytosis. *EMBO J.* **20**, 2202–2213.
- Liscum, L., and Faust, J.R. (1989). The intracellular transport of low density lipoprotein-derived cholesterol is inhibited in Chinese hamster ovary cells cultured with 3-beta-[2-(diethylamino)ethoxy]androst-5-en-17-one. *J. Biol. Chem.* **264**, 11796–11806.
- Luftman, K., Hasan, N., Day, P., Hardee, D., and Hu, C. (2009). Silencing of VAMP3 inhibits cell migration and integrin-mediated adhesion. *Biochem. Biophys. Res. Commun.* **380**, 65–70.
- Mallard, F., Tang, B.L., Galli, T., Tenza, D., Saint-Pol, A., Yue, X., Antony, C., Hong, W., Goud, B., and Johannes, L. (2002). Early/recycling endosomes-to-TGN transport involves two SNARE complexes and a Rab6 isoform. *J. Cell Biol.* **156**, 653–664.
- Maxfield, F.R., and McGraw, T.E. (2004). Endocytic recycling. *Nat. Rev. Mol. Cell Biol.* **5**, 121–132.
- Maxfield, F.R., and van Meer, G. (2010). Cholesterol, the central lipid of mammalian cells. *Curr. Opin. Cell Biol.* **22**, 422–429.
- McMahon, H.T., Ushkaryov, Y.A., Edelmann, L., Link, E., Binz, T., Niemann, H., Jahn, R., and Südhof, T.C. (1993). Cellubrevin is a ubiquitous tetanus-toxin substrate homologous to a putative synaptic vesicle fusion protein. *Nature* **364**, 346–349.
- Mesmin, B., and Maxfield, F.R. (2009). Intracellular sterol dynamics. *Biochim. Biophys. Acta* **1791**, 636–645.
- Millard, E.E., Srivastava, K., Traub, L.M., Schaffer, J.E., and Ory, D.S. (2000). Niemann-pick type C1 (NPC1) overexpression alters cellular cholesterol homeostasis. *J. Biol. Chem.* **275**, 38445–38451.
- Millard, E.E., Gale, S.E., Dudley, N., Zhang, J., Schaffer, J.E., and Ory, D.S. (2005). The sterol-sensing domain of the Niemann-Pick C1 (NPC1) protein regulates trafficking of low density lipoprotein cholesterol. *J. Biol. Chem.* **280**, 28581–28590.
- Möbius, W., van Donselaar, E., Ohno-Iwashita, Y., Shimada, Y., Heijnen, H.F., Slot, J.W., and Geuze, H.J. (2003). Recycling compartments and the internal vesicles of multivesicular bodies harbor most of the cholesterol found in the endocytic pathway. *Traffic* **4**, 222–231.
- Muller, P.A., Caswell, P.T., Doyle, B., Iwanicki, M.P., Tan, E.H., Karim, S., Lukashchuk, N., Gillespie, D.A., Ludwig, R.L., Gosselin, P., et al. (2009). Mutant p53 drives invasion by promoting integrin recycling. *Cell* **139**, 1327–1341.
- Murray, R.Z., Kay, J.G., Sangermani, D.G., and Stow, J.L. (2005). A role for the phagosome in cytokine secretion. *Science* **310**, 1492–1495.
- Nishimura, T., Uchida, Y., Yachi, R., Kudlyk, T., Lupashin, V., Inoue, T., Taguchi, T., and Arai, H. (2013). Oxysterol-binding protein (OSBP) is required for the perinuclear localization of intra-Golgi v-SNAREs. *Mol. Biol. Cell* **24**, 3534–3544.
- Ohgami, N., Ko, D.C., Thomas, M., Scott, M.P., Chang, C.C., and Chang, T.Y. (2004). Binding between the Niemann-Pick C1 protein and a photoactivatable cholesterol analog requires a functional sterol-sensing domain. *Proc. Natl. Acad. Sci. USA* **101**, 12473–12478.
- Pellinen, T., and Ivaska, J. (2006). Integrin traffic. *J. Cell Sci.* **119**, 3723–3731.
- Pellinen, T., Arjonen, A., Vuoriluoto, K., Kallio, K., Fransén, J.A., and Ivaska, J. (2006). Small GTPase Rab21 regulates cell adhesion and controls endosomal traffic of beta1-integrins. *J. Cell Biol.* **173**, 767–780.
- Pol, A., Martin, S., Fernández, M.A., Ingelmo-Torres, M., Ferguson, C., Enrich, C., and Parton, R.G. (2005). Cholesterol and fatty acids regulate dynamic caveolin trafficking through the Golgi complex and between the cell surface and lipid bodies. *Mol. Biol. Cell* **16**, 2091–2105.
- Powelka, A.M., Sun, J., Li, J., Gao, M., Shaw, L.M., Sonnenberg, A., and Hsu, V.W. (2004). Stimulation-dependent recycling of integrin beta1 regulated by ARF6 and Rab11. *Traffic* **5**, 20–36.

- Proux-Gillardeaux, V., Gavard, J., Irinopoulou, T., Mège, R.M., and Galli, T. (2005). Tetanus neurotoxin-mediated cleavage of cellubrevin impairs epithelial cell migration and integrin-dependent cell adhesion. *Proc. Natl. Acad. Sci. USA* *102*, 6362–6367.
- Ramprasad, O.G., Srinivas, G., Rao, K.S., Joshi, P., Thiery, J.P., Dufour, S., and Pande, G. (2007). Changes in cholesterol levels in the plasma membrane modulate cell signaling and regulate cell adhesion and migration on fibronectin. *Cell Motil. Cytoskeleton* *64*, 199–216.
- Reverter, M., Rentero, C., de Muga, S.V., Alvarez-Guaita, A., Mulay, V., Cairns, R., Wood, P., Monastyrskaya, K., Pol, A., Tebar, F., et al. (2011). Cholesterol transport from late endosomes to the Golgi regulates t-SNARE trafficking, assembly, and function. *Mol. Biol. Cell* *22*, 4108–4123.
- Riggs, K.A., Hasan, N., Humphrey, D., Raleigh, C., Nevitt, C., Corbin, D., and Hu, C. (2012). Regulation of integrin endocytic recycling and chemotactic cell migration by syntaxin 6 and VAMP3 interaction. *J. Cell Sci.* *125*, 3827–3839.
- Roberts, M., Barry, S., Woods, A., van der Sluijs, P., and Norman, J. (2001). PDGF-regulated rab4-dependent recycling of  $\alpha$ v $\beta$ 3 integrin from early endosomes is necessary for cell adhesion and spreading. *Curr. Biol.* *11*, 1392–1402.
- Rodríguez-Pascau, L., Toma, C., Macias-Vidal, J., Cozar, M., Cormand, B., Lykopoulou, L., Coll, M.J., Grinberg, D., and Vilageliu, L. (2012). Characterisation of two deletions involving NPC1 and flanking genes in Niemann-Pick type C disease patients. *Mol. Genet. Metab.* *107*, 716–720.
- Röhrli, C., Meisslitzer-Ruppitsch, C., Bittman, R., Li, Z., Pabst, G., Prassl, R., Strobl, W., Neumüller, J., Ellinger, A., Pavelka, M., and Stangl, H. (2012). Combined light and electron microscopy using diaminobenzidine photooxidation to monitor trafficking of lipids derived from lipoprotein particles. *Curr. Pharm. Biotechnol.* *13*, 331–340.
- Schwend, T., Loucks, E.J., Snyder, D., and Ahlgren, S.C. (2011). Requirement of Npc1 and availability of cholesterol for early embryonic cell movements in zebrafish. *J. Lipid Res.* *52*, 1328–1344.
- Simons, K., and Ikonen, E. (2000). How cells handle cholesterol. *Science* *290*, 1721–1726.
- Simonsen, A., Gaullier, J.M., D'Arrigo, A., and Stenmark, H. (1999). The Rab5 effector EEA1 interacts directly with syntaxin-6. *J. Biol. Chem.* *274*, 28857–28860.
- Skalski, M., and Coppelino, M.G. (2005). SNARE-mediated trafficking of  $\alpha$ 5 $\beta$ 1 integrin is required for spreading in CHO cells. *Biochem. Biophys. Res. Commun.* *335*, 1199–1210.
- Skalski, M., Yi, Q., Kean, M.J., Myers, D.W., Williams, K.C., Burtnik, A., and Coppelino, M.G. (2010). Lamellipodium extension and membrane ruffling require different SNARE-mediated trafficking pathways. *BMC Cell Biol.* *11*, 62.
- Tayeb, M.A., Skalski, M., Cha, M.C., Kean, M.J., Scaife, M., and Coppelino, M.G. (2005). Inhibition of SNARE-mediated membrane traffic impairs cell migration. *Exp. Cell Res.* *305*, 63–73.
- Timpson, P., McGhee, E.J., Erami, Z., Nobis, M., Quinn, J.A., Edward, M., and Anderson, K.I. (2011a). Organotypic collagen I assay: a malleable platform to assess cell behaviour in a 3-dimensional context. *J. Vis. Exp.* *56*, e3089.
- Timpson, P., McGhee, E.J., Morton, J.P., von Kriegsheim, A., Schwarz, J.P., Karim, S.A., Doyle, B., Quinn, J.A., Carragher, N.O., Edward, M., et al. (2011b). Spatial regulation of RhoA activity during pancreatic cancer cell invasion driven by mutant p53. *Cancer Res.* *71*, 747–757.
- Tiwari, A., Jung, J.J., Inamdar, S.M., Brown, C.O., Goel, A., and Choudhury, A. (2011). Endothelial cell migration on fibronectin is regulated by syntaxin 6-mediated  $\alpha$ 5 $\beta$ 1 integrin recycling. *J. Biol. Chem.* *286*, 36749–36761.
- Tran, T.H., Zeng, Q., and Hong, W. (2007). VAMP4 cycles from the cell surface to the trans-Golgi network via sorting and recycling endosomes. *J. Cell Sci.* *120*, 1028–1041.
- Urano, Y., Watanabe, H., Murphy, S.R., Shibuya, Y., Geng, Y., Peden, A.A., Chang, C.C., and Chang, T.Y. (2008). Transport of LDL-derived cholesterol from the NPC1 compartment to the ER involves the trans-Golgi network and the SNARE protein complex. *Proc. Natl. Acad. Sci. USA* *105*, 16513–16518.
- Veale, K.J., Offenhäuser, C., Whittaker, S.P., Estrella, R.P., and Murray, R.Z. (2010). Recycling endosome membrane incorporation into the leading edge regulates lamellipodia formation and macrophage migration. *Traffic* *11*, 1370–1379.
- Veale, K.J., Offenhäuser, C., and Murray, R.Z. (2011). The role of the recycling endosome in regulating lamellipodia formation and macrophage migration. *Commun. Integr. Biol.* *4*, 44–47.
- Wang, Y., Thiele, C., and Huttner, W.B. (2000). Cholesterol is required for the formation of regulated and constitutive secretory vesicles from the trans-Golgi network. *Traffic* *1*, 952–962.
- Wendler, F., and Tooze, S. (2001). Syntaxin 6: the promiscuous behaviour of a SNARE protein. *Traffic* *2*, 606–611.
- Zeng, Q., Tran, T.T., Tan, H.X., and Hong, W. (2003). The cytoplasmic domain of Vamp4 and Vamp5 is responsible for their correct subcellular targeting: the N-terminal extension of VAMP4 contains a dominant autonomous targeting signal for the trans-Golgi network. *J. Biol. Chem.* *278*, 23046–23054.
- Zhang, Y., Shu, L., and Chen, X. (2008). Syntaxin 6, a regulator of the protein trafficking machinery and a target of the p53 family, is required for cell adhesion and survival. *J. Biol. Chem.* *283*, 30689–30698.
- Zylbersztein, K., and Galli, T. (2011). Vesicular traffic in cell navigation. *FEBS J.* *278*, 4497–4505.